Computers & Geosciences 166 (2022) 105142

Contents lists available at ScienceDirect

Computers and Geosciences

journal homepage: www.elsevier.com/locate/cageo

A computer vision algorithm for interpreting lacustrine carbonate textures at Searles Valley, USA

Michaela Fendrock [a,b,*], Christine Y. Chen [a,b,c], Kristian J. Olson [d], Tim K. Lowenstein [d], David McGee [a]

[a] Department of Earth, Atmospheric and Planetary Sciences, Massachusetts Institute of Technology, Cambridge, MA, USA
[b] Department of Marine Geology and Geophysics, Woods Hole Oceanographic Institution, Woods Hole, MA, USA
[c] Chemical and Isotopic Signatures Group, Division of Nuclear and Chemical Sciences, Lawrence Livermore National Laboratory, Livermore, CA, USA
[d] Department of Geological Sciences and Environmental Studies, Binghamton University, Binghamton, NY, USA

ARTICLE INFO

Keywords:
Machine learning
Computer vision
Carbonates
Paleoclimate

ABSTRACT

Investigations of the paleohydrologies of pluvial lake systems have often employed lake carbonate deposits called "tufa" that grow subaqueously and can be preserved long after the drying of the lake. For this reason, tufa have been used as a proxy for minimum lake level. However, they exhibit a variety of textures that hold the potential to reveal richer paleoclimatological information. With the goal of determining if tufa texture can be used as a proxy for lake environment, this study investigates the textures of tufa at Mono Lake, California in comparison to the fossil tufa in Searles Valley, California. While observations in the last century suggest that the tufa in the Mono basin grew in waters similar to the modern, the tufa at Searles formed during the last glacial period, when the Great Basin contained a system of pluvial lakes on the scale of the modern Great Lakes. The tufa at both basins have been observed to have a range of classifiable textures, and new methods of inspecting visual data could be informative about what factors control these textures. To this end, a t-Distributed Stochastic Neighbor Embedding (t-SNE) algorithm is used to project images of the tufa at Searles and Mono into a coordinate space, allowing for simple, quantitative comparisons of the visual similarity of textures. The textures of tufa at Searles are compared to each other, as well as to the tufa at Mono. This study performs a robust assessment of the feasibility of Mono Lake as a modern analogue for Searles Valley. It finds that there is a justifiable basis for the comparison of certain fossil facies at Searles to the tufa at Mono, significant progress towards the goal of using texture as a metric for the environment in which tufa formed.

1. Introduction

As remnants of a wetter time, enigmatic deposits called tufa have been used as proxies for lake level in closed basin lakes. To first order, these deposits are known to have grown subaqueously. If they are found in a known or suspected lake system, they can be used to assign a minimum lake depth. That is, where tufa are found, there must once have been water. Along these lines, they have been dated using U/Th and radiocarbon dating, constraining the time when the observed lake level was reached (e.g. Broecker and Orr, 1958; Kaufman and Broecker, 1965; Candy and Schreve, 2007). As carbonate deposits, tufa also hold significant potential for gleaning information about lake chemistry (e.g. $\delta^{18}O$, biological activity, Guo and Chafetz, 2014; Petryshyn et al., 2016)). But with greater exploration, there is reason to believe that tufa hold more paleoclimatological information than simply lake chemistry. Depending on the mechanism of their formation, the presence of tufa could also be revealing of specific environmental factors. For example, if the precipitation of tufa was dependent on the presence of phototrophic organisms, tufa would only form shallow enough in the lake that light could penetrate (i.e. the photic zone), limiting the possible range of depths where tufa could grow (DeMott et al., 2020). Alternatively, inorganic precipitation of the tufa may require that the lake have a high alkalinity and an input of Ca ions (e.g. from springs). Gleaning the signature of these mechanisms in the geologic record would thus broaden the potential use of tufa as paleolake proxies. Tufa are found in a number of modern lakes in the United States and elsewhere (e.g. Green Lake, Pyramid Lake, Mono Lake), as well as in paleolakes that are now at significantly lower levels or fully dry (e.g. Lake Bonneville, Lake Manly, Searles Lake) (Ford and Pedley, 1996; Ku et al., 1998; Guo and Chafetz, 2012; DeMott et al., 2020).

* Corresponding author at: Department of Earth, Atmospheric and Planetary Sciences, Massachusetts Institute of Technology, Cambridge, MA, USA.
E-mail address: mfend@mit.edu (M. Fendrock).

https://doi.org/10.1016/j.cageo.2022.105142
Received 9 July 2021; Received in revised form 9 May 2022; Accepted 12 May 2022
Available online 25 May 2022

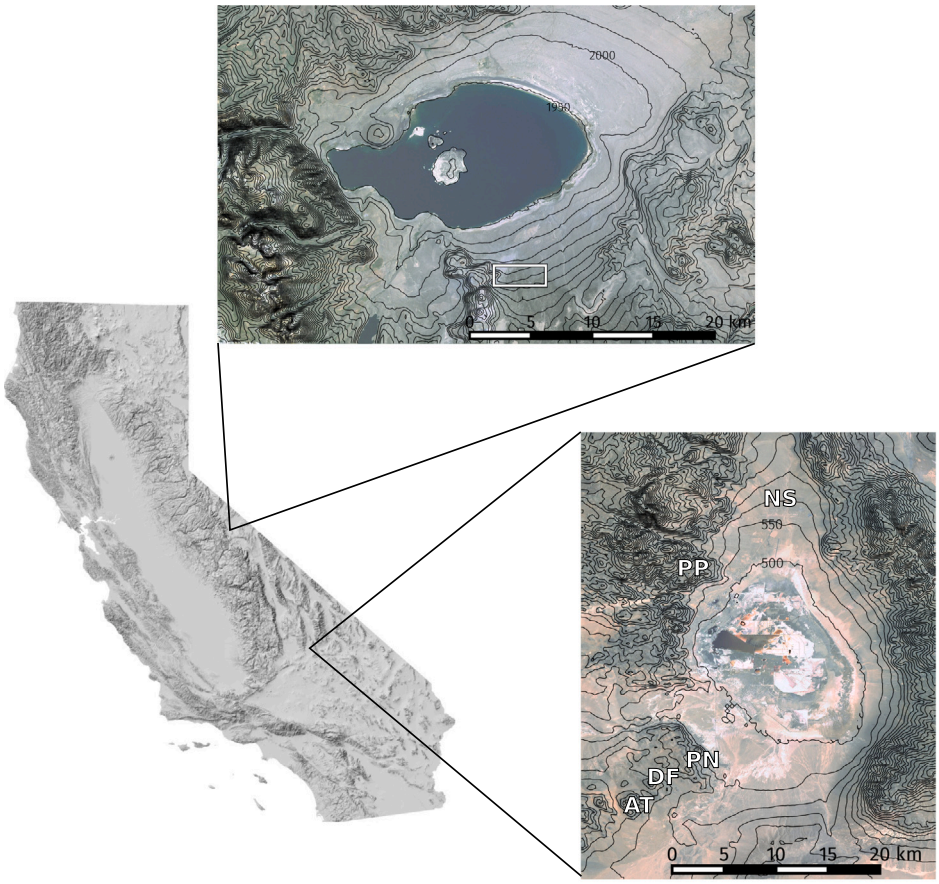

Fig. 1. Locations of basins considered in this study: Mono Lake (north) and Searles Valley (south). Locations of tufa considered in this study are indicated by a white box at Mono Lake and by labeling of sites at Searles Valley. Contours are at 50 m intervals of meters above sea level.

Both preserved and relatively modern tufa exhibit a range of primary, centimeter-scale textures (e.g. Dunn, 1953; Guo and Chafetz, 2012). Even within a basin, it is likely that tufa formed in different environments in terms of chemistry, depth, biology, temperature, or some combination of these factors: changes that may be reflected in the primary texture of the tufa (Shearman et al., 1989; Benson, 1994). An avenue for exploring this connection could be to make comparisons of fossil tufa to modern tufa, whose growth environment is better understood. Traditional methods such as field comparisons and petrographic observations may be fruitful in these efforts. At Searles Valley, microscopic examinations of the micrometer scale structure of tufa suggested the possibility of microbial or bacterial involvement in the construction of tufa, but could not determine the degree to which such biology was necessary for tufa growth (Guo and Chafetz, 2012). Similarly, microscopic inspection of the tufa at Mono find evidence for microbes living on the tufa, but suggest also that the majority of tufa is precipitated inorganically (Brasier et al., 2018). Indeed, earlier studies of the tufa at Mono found evidence for a purely abiotic precipitation mechanism for the tufa at Mono, driven by mixing of spring and lake waters (Bischoff et al., 1993). Thus, while it is likely that the tufa at Mono was precipitated abiotically, ambiguity remains about the tufa at both of these basins, and new tools may provide valuable perspectives.

To this end, it has been demonstrated that machine learning has the ability to uncover nuances in data sets that are too subtle or complicated for human researchers (e.g. Pérez-Ortiz et al., 2019; Fang and Li, 2019; Huntingford et al., 2019). With relative ease, machine learning can thoroughly evaluate a data set, while at the same time rigorous computational iteration allows for confidence that the best solution has been found. A form of this, the field of computer vision is concerned with using computers to better understand visual data such as digital images.

Here, a computer vision algorithm is used to objectively classify tufa textures in two closed basins lakes: Searles Valley, CA and Mono Lake, CA (Fig. 1). Closed basin lakes are basins with no outflows. As a result, the level of these lakes depends on the difference between precipitation into the lake or its inflows, and evaporation out of the lake (P – E). Studies have attempted to solidify the relationship between past climate and paleolake level using hydrological balance models (e.g. Hostetler and Bartlein, 1990), however these efforts are limited by knowledge of past lake level. If evidence of the depth of a closed basin lake can be gleaned from the geologic record, it can be used to constrain modeling efforts. This work assesses the utility of computer vision as a complement to more traditional, field-based geologic investigations. It also investigates the relationship between computer vision-based classifications of tufa texture and environment, including an assessment of the comparability of the better understood Mono Lake tufa to the fossil tufa in Searles Valley. Specifically, a machine learning algorithm is used to compare tufa textures found within Searles and Mono to ask the following questions: **(1)** Is a particular facies of tufa at Searles objectively visually similar to those at Mono? And **(2)** Can the variance of tufa textures at Searles Valley, CA be tied to their elevation – perhaps corresponding to instances of comparable lake conditions or background climate?

1.1. Areas of study

1.1.1. Searles valley

During the late Pleistocene, the drainage from the Sierra Nevada flowed through the Owens River into Owens Lake (Peng et al., 1978, Fig. 1). When P - E was high enough, Owens Lake would overflow into China Lake, which, with sufficient precipitation, would in turn

overflow into Searles. The chain would continue with Panamint Lake and then Lake Manly (present-day Death Valley, Jayko et al., 2008). When Searles did not overflow, it was the terminus of the drainage and could be considered a true closed basin lake. This was the case for much of the lake's history, and during these times its level was an indicator of the up-stream hydrology of the lake system described above (Smith, 2009). The lake level history of Searles is thus of great interest for deciphering the hydroclimate of the Great Basin in the Late Pleistocene. Past studies gleaned past lake level by inferring relative lake depth from salts in sediment cores, revealing a history of dramatic lake level change (Smith, 2009). However, shoreline studies are necessary to accurately determine the magnitude of lake level change and constrain the true depths that the lake reached in its past.

In addition to sediment cores, past researchers have used the extensive tufa deposits at Searles to investigate its hydrological past. The tufa in Searles Valley exhibit a variety of morphologies and textures from the almost 50 m tall Pinnacles in the south of the basin to the more localized mounds higher on the shores of the paleolake (locations shown in Fig. 1). In studies based in the Pinnacles, the Searles tufa offer a distinctive stratigraphy (Scholl, 1960; Guo and Chafetz, 2012). The four reported facies are: porous, nodular, and columnar tufa; and finely laminated crusts (Fig. 2). The porous tufa are the most common in north and central parts of the Pinnacles, and exhibit a somewhat open texture with subplanar fabrics, resembling the exterior of a wasps' nest. From stratigraphic context, Guo and Chafetz (2012) suggest that one interval of porous tufa is believed to be the youngest deposit in the Searles tufa, and another is believed to be the oldest. The nodular tufa overlay the older porous tufa layer and occur most commonly in the northern Pinnacles. They have a popcorn-like texture and are composed of multiple generations. The columnar tufa overlay the older porous tufa and occur most commonly in the middle group. They resemble asparagus bunches and are found in various states of weathering. The finely laminated crusts areas described, and are found draping either the nodular or columnar tufa. The stratigraphy defined by Guo and Chafetz (2012) at the Pinnacles is thus (from inner to outer/oldest to youngest): older porous tufa, columnar or nodular tufa (depending on part of the basin), finely laminated crust, younger porous tufa. The finely laminated crusts are not considered in this study, as the exposure of this facies is too limited to produce an adequate sample size.

Despite this well defined stratigraphy, the mechanism and conditions surrounding the formation of the tufa and its various facies are not well known. While some deposits are reasonably interpreted as "shoreline" (i.e. shallow) tufa, others, such as the Pinnacles, seemingly must have formed at significant depth. The usefulness of these deposits could thus be improved with a better understanding of how they formed as well as what controls the observed variability of texture. Should the variety of textures seen in tufa prove to correspond to a particular depth or chemical regime in the lake (e.g. saturation state), the carbonate deposits could be used to more precisely constrain lake level and environment at the time of deposition. Comparison of the variability of tufa textures within Searles Valley will address the second question posed above: does the variability of the textures of tufa in Searles correspond to their elevation in the basin?

1.1.2. Mono lake

Mono Lake is north of Searles in the Eastern Sierra Nevada. Mono is in a structural basin of the Eastern Sierra, a tectonically and volcanically active area (Stine, 1990). Also a closed basin lake, the level of Mono reflects the drainage of the Eastern Sierra. During the late Pleistocene, a larger lake known as Lake Russell filled the Mono basin (Benson et al., 1990). Like most other Great Basin lakes, the most recent highstand in the Mono basin occurred during Heinrich stadial 1 (Munroe and Laabs, 2013). Records of higher lake-level can be found in shoreline features at high elevation in the basin, cores from the lake, and other geomorphic evidence including stream cuts through deltas and other lacustrine deposits (Stine, 1990).

At Mono Lake, the interaction of Ca^{2+} rich spring water with the carbonate-rich lake water contributes to the growth of tufa (Dunn, 1953; Scholl and Taft, 1964; Council and Bennett, 1993). These tufa are home to algal communities that are believed to promote their growth, though not significantly enough to classify them as "microbialites" (Scholl and Taft, 1964; Brasier et al., 2018). Indeed, the saturation state of water is believed to be the primary driver of the deposition of tufa at Mono Lake (Council and Bennett, 1993). One mechanism for their formation would be that spring water percolates through the shaft of the tufa and is discharged from the top, and carbonate is precipitated on the outside of the structure (Scholl and Taft, 1964). The diversion of Eastern Sierra water by the Los Angeles Aquaduct lowered Mono Lake's level by almost 15 m, exposing tufa along much of the lake's shoreline (Vorster, 1985). The Mono Lake tufa can thus be explored in detail from land, though the lake is believed to still be actively forming the deposits, a process that has been observed visually within the last century (Dunn, 1953; Bischoff et al., 1993). Previous researchers (e.g. Dunn, 1953) have noted the presence of 3–4 facies of tufa, with more porous tufa deeper in the lake or at its shore, and more dense, nodular-type tufa above shore (i.e. from a time when lake level was higher). These facies were not necessarily observed or captured in this study. However, given that past workers had access to the North Shore of Mono Lake (which was not accessible for this study), it is reasonable to expect that the range of tufa seen at Mono Lake in this study is smaller than that of previous studies. Likewise, the tufa available for inspection to this study were all at approximately the same elevation (modern lake level), thus a within-basin comparison of tufa texture to elevation was not possible.

Comparison of the tufa observed at Mono Lake will address the first question posed above: how do the tufa at Searles compare visually to the tufa at Mono? How does this comparison inform the interpretation of the environment in which the Searles tufa formed?

2. Methodology

Data for this project were collected during field seasons in October of 2018 at Searles and Mono Lakes, and January 2020 at Searles. The data set consists of ~1500 images collected of the textures of the tufa at the two lakes. Photo sites were chosen by exposure: all outcrops available and accessible in Searles and Mono were photographed. Photos were taken where textures were best exposed: this means that nodular and porous tufa were imaged in planform, whereas columnar tufa were imaged in cross section. It is possible that this difference could introduce unexpected biases to the results of this study. However, the orientation of images in cross-section or planform was an unavoidable limitation of how the textures were exposed.

The field of view captured in these images varied somewhat in size, but were ~10 cm across (scale bar later removed for processing). In collecting images, effort was taken to maintain uniform lighting (e.g. by shadowing on particularly bright days) and to avoid major, non-primary textural features such as cracks or plant overgrowth. The data processing of this project was performed in four parts, discussed in greater detail below: (1) the data were preprocessed to normalize for visual and structural similarity, (2) A t-SNE algorithm was applied to the images to reduce the dimensionality of the data, (3) a k-means clustering algorithm was used on the results of (2), and (4) clusters from part (3) were compared to environmental data (e.g. elevation, locality). These steps reduced the data from raw field images into data points that could be more easily numerically manipulated in later steps, and compared to each other in a quantitative manner.

2.1. Pre-processing

Images were pre-processed with the goal of eliminating all features irrelevant to the textures pictured. The information of color and lighting were not relevant to the goal of the algorithm: to classify

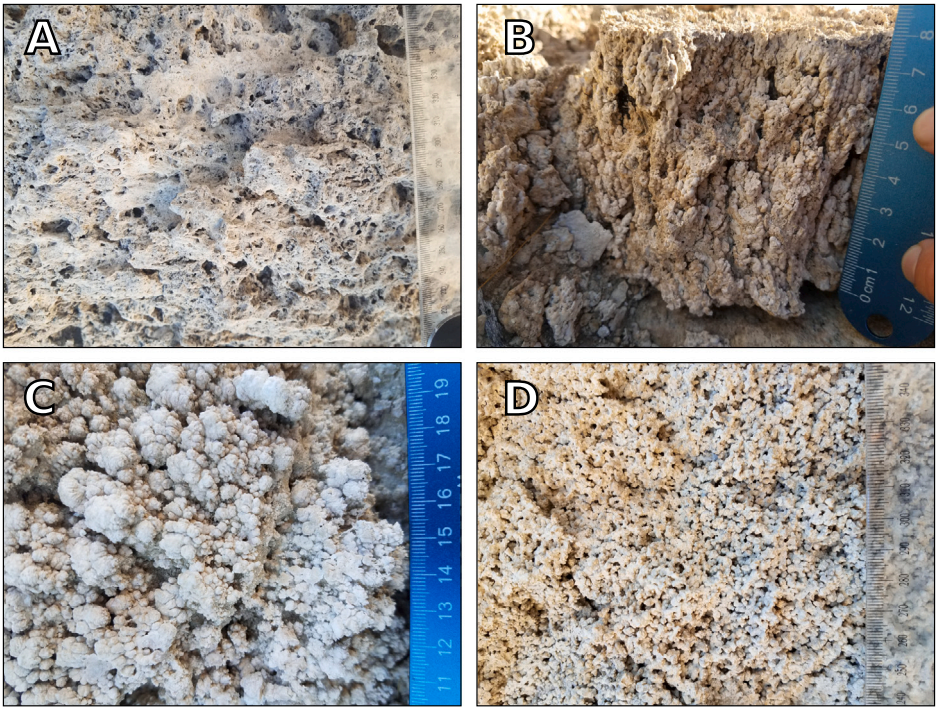

Fig. 2. Examples of the endmember facies relevant to this study: (A) Porous tufa, (B) columnar tufa, (C) nodular tufa with well defined, popcorn-like baubles, and (D) a more weathered example of nodular tufa.

the variability of the textures in the tufa. Thus, all pre-processing was in effort to normalize images across these parameters (Fig. 4). Images were considered to be on a reasonably comparable scale as collected, so scale bars were cropped out and no further steps were taken to normalize scale. Then, all images were converted to grayscale to remove color effects. Though the tufa are broadly similar in color, there is a possibility of differences between images due to lighting effects and camera white balance. The image histogram was then equalized to remove remaining lighting effects. Though effort was made in the field to have uniform lighting in images, this was not always possible. To minimize the possibility of the algorithm clustering on lighting effects (rather than actual geologic information), histogram normalization brightens darker areas in the image and darkens lighter ones creating the effect of uniform lighting. Finally, the t-SNE algorithm used here requires image inputs of uniform size. Thus, images were trimmed to the size of the smallest image in the data set after the scale was removed. Trimming was done from the edges to retain the center of the image, where the image taker would have directed their focus.

2.2. Machine learning algorithms

2.2.1. t-Distributed Stochastic Neighbor Embedding

t-Distributed Stochastic Neighbor Embedding (t-SNE) is an algorithm used to transform complex, high-dimensional data sets into a more manageable space of 2 or 3 dimensions (Van der Maaten and Hinton, 2008). In addition to Uniform Manifold Approximation and Projection (UMAP), t-SNE has become one of the standard algorithms for managing high dimensional data by projecting it into lower dimensions, both are used commonly in health care applications (e.g. Abdelmoula et al., 2016; Li et al., 2017; Kobak and Berens, 2019), and increasingly in the Earth sciences (e.g. Klimczak et al., 2020; Njock et al., 2020). In direct comparisons, UMAP and t-SNE have been found to have similar results (Becht et al., 2018; Kobak and Linderman, 2019). This study uses t-SNE, but it is expected similar results would be found using UMAP. Other algorithms exist for comparing the similarity of images (e.g. Convolutional Neural Nets, Artificial Neural Nets), but this study focuses solely on the effectiveness of t-SNE.

As mentioned above, the specific function of these algorithms is to project complicated, high-dimensional data into a more manageable space. Though images are often (and not incorrectly) thought of as two-dimensional, in the case of digital images, their dimensionality can also be considered equal to the number of pixels. In this case, each pixel is a vector with magnitude equivalent to the pixel's color value. When plotting digital image data in this space, the relative location of the images will correspond to where the variability within the images lies: their visual similarity (Alfeld et al., 2018; Pouyet et al., 2018; Linderman and Steinerberger, 2019). However, as this space has a number of dimensions equal to the number of pixels in each image, working with data in this way is extremely difficult. t-SNE allows for the projection of data from higher dimensions into two dimensions, where they can be more easily manipulated. The projection step maintains the relative distance of data points to each other and thus also maintains the overall structure of the data set (Linderman and Steinerberger, 2019).

In the implementation of t-SNE in this study, each image is considered an object and each pixel in the image is considered a dimension of that object. A probability ($p_{i|j}$) of similarity between objects (e.g. x_i and x_j):

$$p_{i|j} = \frac{exp(-\|x_i - x_j\|^2/2\sigma_i^2)}{\Sigma_{k\neq i} exp(-\|x_i - x_k\|^2/2\sigma_i^2)} \quad (1)$$

where σ is the variance of a Gaussian surrounding object x_i. This Gaussian is computed depending on the parameterization of t-SNE, and has a larger bandwidth where the spread of the data is greater. Considering N objects, the probability p_{ij} is computed from the above values as:

$$p_{ij} = \frac{p_{j|i} + p_{i|j}}{N} \quad (2)$$

p_{ij} is thus the probability that x_i and x_j would be neighbors if all objects in the set were lined up by similarity (p_{ii} is set to zero). The algorithm then learns a map with corresponding points (i.e. y_i, y_j) that represent the similarities in p_{ij}. From this space, the probability of similarity

Fig. 3. Comparable textures at Searles (left) and Mono (right), as well as similar large-scale structures (bottom row). The "towers" found at Searles (such as those shown here) are found most commonly at the Amphitheatre site, which was found to have the highest proportion of columnar tufa.

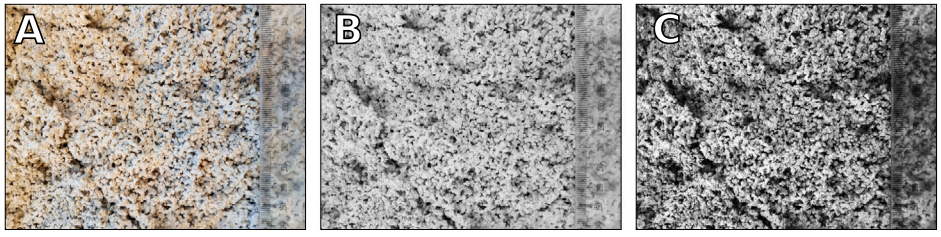

Fig. 4. Steps in preprocessing tufa images: (A) Original image (scale bar left for reference in this paper but would otherwise be removed), (B) image converted to grayscale to avoid color effects (e.g. the orange on the left of the original image), and (C) equalizing of image histogram for uniformity of shading. This step has the added benefit of emphasizing the textures pictured. (For interpretation of the references to color in this figure legend, the reader is referred to the web version of this article.)

between y-space points (q_{ij}) is computed:

$$q_{ij} = \frac{(1 + \|y_i - y_j\|^2)^{-1}}{\Sigma_{k \neq i}(1 + \|y_i - y_k\|^2)^{-1}} \tag{3}$$

q_{ii} is also set to zero. Finally, the locations on the final map are found by reducing the Kullback–Leibler divergence of the distribution of Q from that of P using gradient descent:

$$KL(P \parallel Q) = \sum_{i \neq j} p_{ij} log \frac{p_{ij}}{q_{ij}} \tag{4}$$

In the resulting data, objects are projected from their higher dimensional space into two dimensions. In simplest terms, the t-SNE algorithm calculates distances between objects in a high dimensional space. It then iteratively organizes objects in lower dimensional space, so that their relative distances are the same as (or as close as possible to) in their original higher dimensionality.

In this implementation, the "distances" are calculated based on the grayscale pixel values of the data, so the distances between objects should correlate to their visual similarity. Each object began with a dimensionality equal to the number of pixels, and ended as a 2-D object, each dimension a value between zero and one. When plotted by these dimensions, with the Euclidean distances between points proportionate to the visual similarity between corresponding images, we are able to observe the similarity of images as numerical data and view once qualitative relationships, quantitatively.

Table 1
Parameterizations that were run on the full data set, after testing on a representative subset. Bottom row (bold) was ultimately used for the analysis below.

Perplexity	Number of Iterations
17	250
19	250
9	250
19	3000
20	250
18	**20,000**

2.2.2. k-means

An unsupervised k-means clustering algorithm was then applied to each set of images corresponding to the basins (Mono and Searles). k-means clustering seeks to sort a data set into k clusters by similarity, with the Euclidean distances between clusters relating to the similarity between them (Pedregosa et al., 2011). In this study the k-means clustering was applied to the two dimensions resulting from the t-SNE algorithm, with the dimensions corresponding to visual similarity (Celik, 2009). The parameter k (the prescribed number of clusters) was set to three to correspond to the hypothesized number of facies (nodular, columnar, porous). A sensitivity analysis of the value of k is provided in the appendix.

Following the clustering of images from Searles alone, the algorithm was then run on the full combined set of images, determining the best clustering for the full data set including the images from Mono. A machine learning technique such as this is favored for its objectivity in image comparison, as well as the relative facility with which it can process 1500+ images (Kanungo et al., 2002).

2.2.3. Choice of parameters

Two parameters are adjustable when using t-SNE: the number of iterations the algorithm goes through, and the perplexity. The algorithm "learns" each time it iterates through the steps defined above. One must then allow it enough "tries" to learn how to best project the data into a smaller dimensional space. However, too many iterations will make the algorithm unnecessarily slow. Perplexity is a measure of how the algorithm should weigh the similarity of neighboring data points as compared to the data set on a whole (Wattenberg et al., 2016). Since the nature of the clustering of the data was not well understood a priori, multiple parameterizations were tried to determine which would be best suited to the data. First, the algorithm was run on a representative subset of 20 images with each combination of perplexity 1–20 and for iterations of 250, 500, 1000, 2000, 3000, 5000, 7000, 10000, and 20000, with the intention of narrowing down the best possible parameterization while optimizing computing time. From these results, the algorithm was then run on the full data set using the parameterizations defined in Table 1.

For each of these t-SNE parameterizations, k-means clustering was performed and a number of clustering metrics were computed (Silo score, Calinski score, Davies Bouldin index; (Palacio Niño and Berzal, 2019)). Unfortunately, the t-SNE parameterizations that were able to produce the k-means clusterings with the best metrics, also were interpreted as demonstrating artifacts of overfitting, including elongated mapping into lower dimensional space, as if points were plotted along a line (Wattenberg et al., 2016). Thus, the t-SNE parameterization with the least appearance of overfitting was chosen, a perplexity of 18 with 20,000 iterations, though its clustering metrics were relatively unfavorable. The realization that while the resulting clusters were less tight or separated, they generally contained the same set of points instilled confidence in this choice of parameters.

Table 2
General distribution of facies between clusters. The right column ("20 endmembers") shows the division of the 20 images from each cluster that plotted farthest from the mean image of the whole data set. The process for this selection is described in-text. Examples of the textures described here can be found in Fig. 2.

Cluster Number	Facies	*20 endmembers*
1	Weathered nodular	*11 weathered nodular, 9 porous*
2	Columnar	*7 columnar, 13 porous*
3	Nodular	*2 weathered nodular, 9 nodular, 9 porous*

3. Results

The products of the t-SNE and k-means algorithms on the Searles data alone as well as with Mono data are shown in Fig. 5. The clusters found by k-means abut each other and are not separated by space. If the clusters found by k-means are defined by visual similarity, they ought to each correspond to the three facies defined by Guo and Chafetz (2012, nodular, columnar, porous), which were also defined by visual similarity. Images in each cluster were manually inspected to determine which facies were most common in each cluster — the result of this inspection can be found in Table 2. Porous tufa were distributed approximately evenly between clusters, seemingly not recognized as a separate facies. Rather, the more weathered facies, particularly the weathered nodules shown in Fig. 2, were mostly in cluster 1 with some porous images. Cluster 2 was primarily the columnar tufa, with porous tufa that had a more elongate texture. Similarly, cluster 3 was nodular tufa with porous tufa with a somewhat nodular-like texture. None of the clusters excluded any of the facies, but roughly maintained the groupings described here with proportionally more of the relevant facies. Images of porous tufa were evenly distributed between clusters, likely because the texture of the porous tufa can at times appear like that of the other facies. Thus, in the following discussion the porous tufa will be ignored and the clusters will be referred to by the other facies they contained (per 2).

To confirm the facies assignments, the 20 images that plotted the furthest from the center of all the clusters were found for each cluster. That is, all three clusters are plotted on axes that range from 0–1 in x and y: the 20 points for each cluster were the farthest from the coordinate (0.5, 0.5). These points should be farthest from the "average image" for the whole data set, which would plot at (0.5, 0.5), and should thus be "endmember examples" of each cluster. A facies was then assigned to the set of 20 from each cluster. About half of each set of 20 were images of porous tufa, but the rest were as described above (cluster 1: weathered nodular, cluster 2: columnar, cluster 3:nodular). The results of this analysis are described in Table 2.

Black points in Fig. 5 are the images collected at Mono Lake. Their distribution demonstrates that the textures of Mono overlap well with those at Searles, indicating that it is not necessary to consider them to be a separate facies from Searles. Likewise, the distribution of Searles data between clusters did not change with the inclusion of the Mono Lake data. That is, the addition of the Mono data did not significantly skew the distribution of clusters. This confirms a general observation in the field that the Mono Lake tufa are visually comparable to some tufa found at Searles.

The distribution of clusters between basins shows a marked preference for columnar tufa at Mono Lake and for weathered nodular tufa at Searles (Fig. 6). The remaining images are approximately evenly distributed between the other two clusters at each basin, but with slightly more nodular tufa at Mono and slightly more columnar tufa at Searles. Almost half of the images from each basin are in the dominant cluster.

The clustering of images collected at Searles was compared to the spatial and elevational distribution of those images (Fig. 8). Despite the >200 m spread in the elevation of data collected at Searles, no real elevation dependence can be observed between tufa facies. The

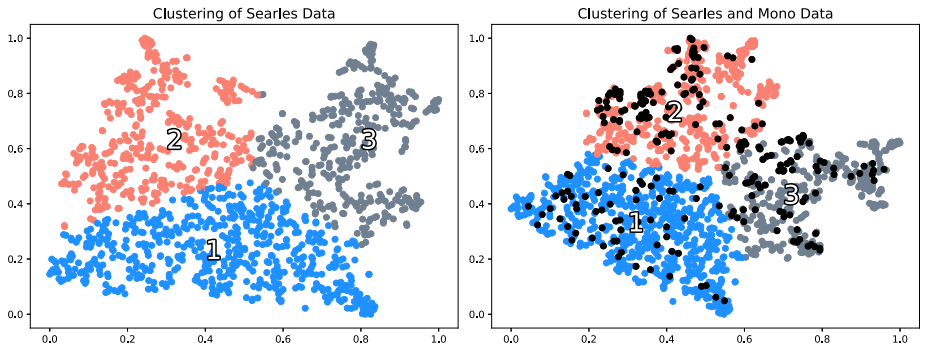

Fig. 5. Clusters found by k-means, clustering on the output of the t-SNE algorithm for (left) the images taken at Searles Valley and (right) the images taken at both Searles and Mono Lake. The 0–1 scale on each axis is dimensionless, the output of the t-SNE algorithm. Nominally, the Euclidean distance between points corresponds to their visual similarity. Points plotted in black are the Mono Lake data. Note that the plot on the right is approximately equivalent to the left plot rotated by ~ 45° clockwise.

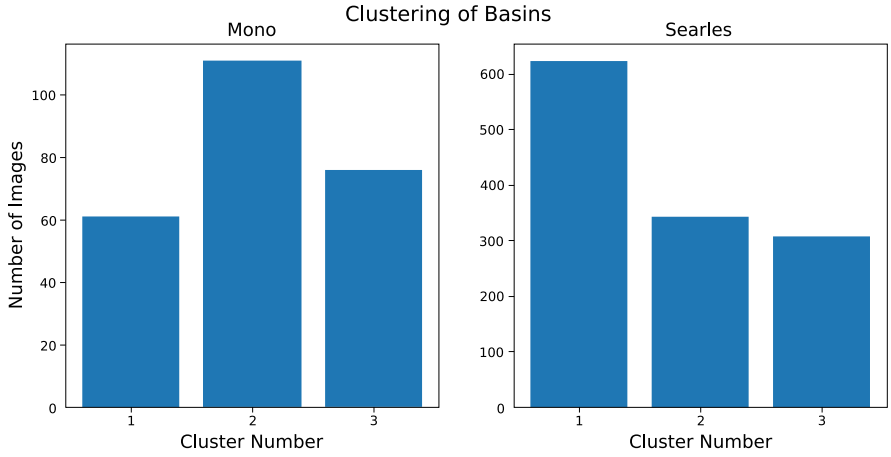

Fig. 6. Distributions of each cluster by basin. Mono is skewed towards cluster 2 (columnar), while Searles is skewed towards cluster 1 (weathered nodules).

latitudinal and spatial distribution of clusters were also considered (Fig. 8). Latitude and field site were treated as separate variables to allow for inspection of local effects such as the exposure of a site (i.e. sheltered from the wind versus exposed to wave action). There is not a strong relationship between the clusters found in this study and latitude/field site. Roughly, though, columnar tufa tend to be more common south in the basin, whereas nodular is proportionally more northern. The northern sites (North Shore and Pioneer Point) have on average 46% nodular and 19% columnar, whereas the southern sites (Amphitheatre, Desperate Forest, and Pinnacles) have on average 22% nodular and 40% columnar.

Nodular tufa is generally found more commonly at the site referred to as "Pioneer Point". Weathered nodular and columnar tufa are found at the site referred to as "the Amphitheater" (Fig. 7). Indeed, the Amphitheatre is the only site at Searles with more than 50% of images falling in the "columnar" classification. This is notable, as the Amphitheater is the site in Searles with the most prominent and well-preserved "towers", structures similar to those found at Mono where columnar tufa was also the dominant facies (Fig. 3).

4. Discussion

The poor clustering of the results of the t-SNE projection could be attributed to a number of factors. First, the processes (e.g. biotic or abiotic precipitation of carbonate) producing end-member tufa textures could be acting at the same time most cases, producing intermediate textures. For example, it is possible that subsequent generations of tufa do not fully erase past textures, and instead work over them. It was observed in the field that columnar tufa may appear to grade into nodular as a primary texture (i.e. not as an effect of weathering). This is not mutually exclusive with the observation of Guo and Chafetz (2012) that these textures are distinct in different regions of the Pinnacles. Rather, it suggests that these facies could be coeval, but variations of lake conditions lead to different morphological expressions. It is also possible that the poor clustering of the data could be a result of a failure or poor parameterization of the t-SNE algorithm. However, this seems unlikely given the number of parameterizations that were tested.

Since cluster 1 seems to be a primarily weathered facies, the dominance of cluster 1 at Searles could simply be because the tufa there are older, and thus more likely to be weathered. However, a statistical basis for correlating tufa texture to elevation could not be found. Thus, this study finds the answer to question (2) above ("Can the variance of tufa textures at Searles Valley, CA be tied to their elevation – perhaps corresponding to instances of comparable lake conditions or background climate?") is that the variance of tufa textures at Searles Valley, CA cannot be tied to their elevation in the basin.

The preponderance of columnar tufa at Mono Lake could indicate that the process responsible for producing this facies dominates tufa production at Mono Lake. Precipitation of tufa at Mono Lake is believed to be a primarily abiotic process, the result of spring discharge into the lake (Council and Bennett, 1993). Also relevant to this comparison is the result that columnar tufa is the most common facies at Mono, as well as at the Amphitheater in Searles. As mentioned above, the Amphitheater at Searles is notable for the tufa "towers" that are prevalent there. These towers are found elsewhere in Searles, but are most common at the Amphitheater. Interestingly, Mono's second most prevalent facies, the nodular tufa, is the dominant facies at Pioneer Point, a site where towers can also be found. The co-occurrence of these facies, especially the columnar tufa, with towers could indicate that the towers at Searles (of unclear origin) are the product of processes similar to those working at Mono (i.e. spring discharge).

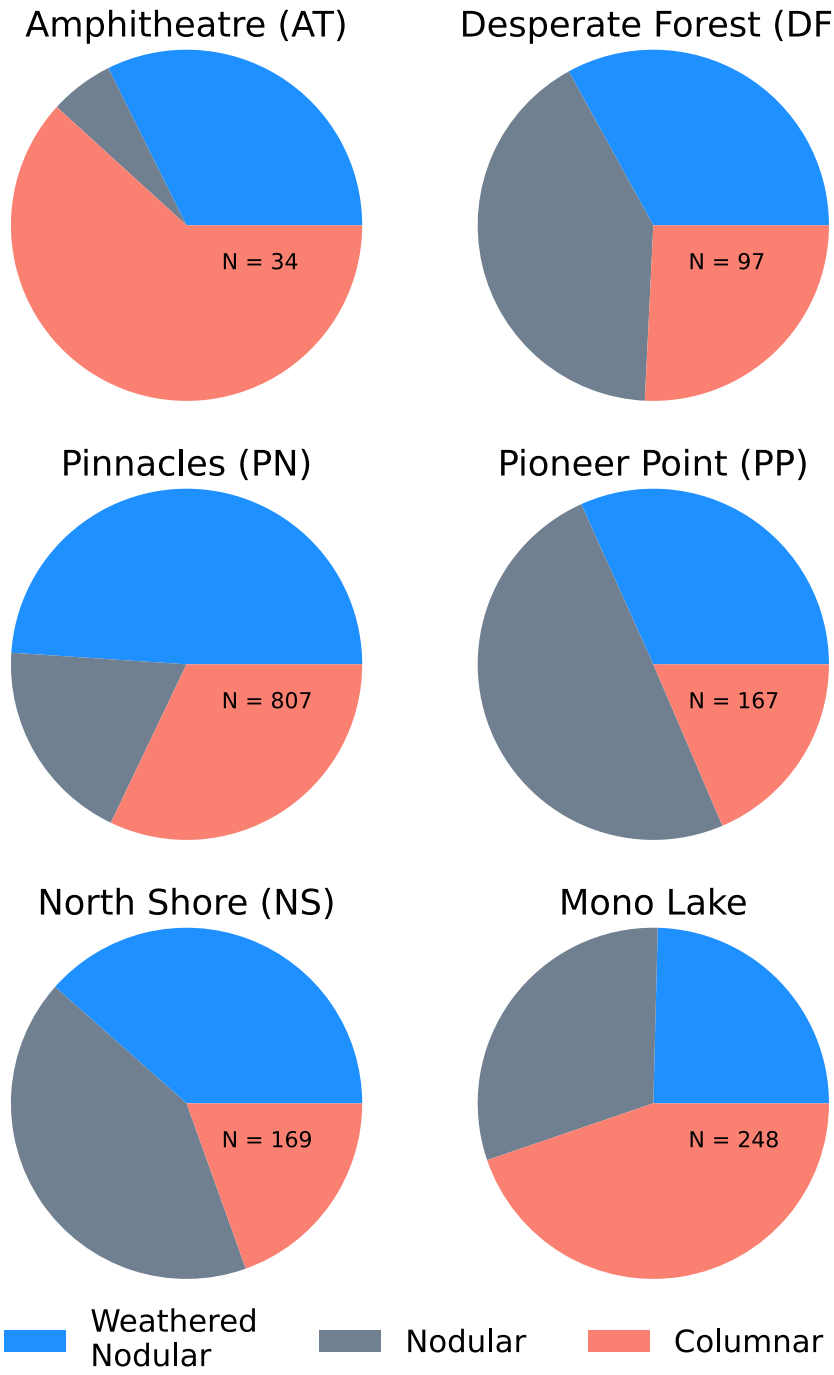

Fig. 7. Distribution of facies within sites. The Amphitheater has the highest proportion of columnar tufa and is the only Searles site with more than 50% columnar. Mono Lake similarly had proportionally more columnar tufa (Fig. 6).

5. Future work

In this study, t-SNE is used largely as an unsupervised algorithm. That is, all the data are used together to allow the algorithm to find a "best" (most statistically defensible) solution; there does not exist a "training set" of data from which the algorithm learns. Since one of the aims of this work was to determine if t-SNE was able to find the same set of facies as human researchers, it was not considered necessary or even favorable to use a supervised algorithm. However, in light of this study, it would be worthwhile to compare the results found here to the facies defined by humans on the same data set. Such an effort would direct future work to refine the t-SNE and k-means algorithms for use on tufa data sets. It would likewise be of interest to compare the results of this study to the same analyses performed using different algorithms (e.g. UMAP, Convolutional Neural Nets, Artificial Neural Nets, etc.). This work demonstrates the utility of just one algorithm, and expanding to others would allow for more robust interpretations of tufa textures and their contexts.

While this study uses a "large" data set of 1500+ images, machine learning algorithms almost always benefit from more data. A conclusion of the January 2020 field campaign was that (short of the discovery of new outcrops) further imagery is not necessary from Searles, as images have been collected of virtually all outcrops. However, future works could improve this effort by collecting more images from Mono Lake. An even richer study could include data from other basins with tufa grown in waters with a distinct chemistry such as Bonneville Basin,

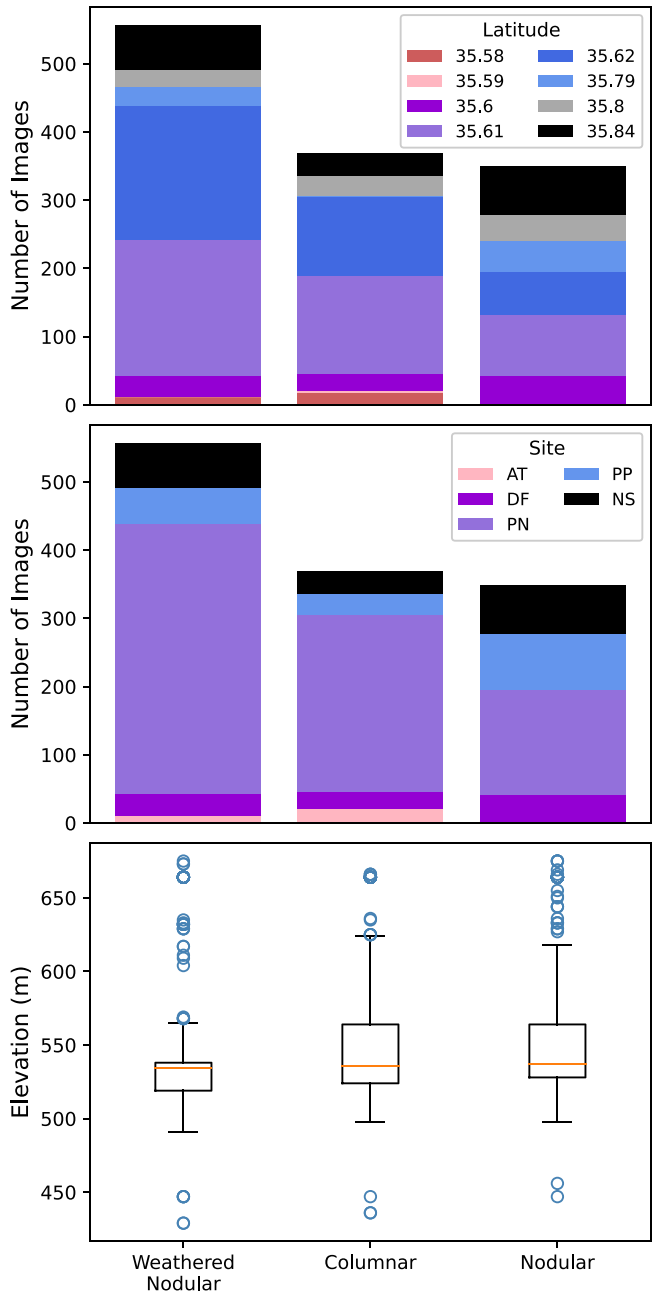

Fig. 8. Comparison of Searles clusters to environmental data. In the top panel, images are binned into hundredths of a degree bins. In the bottom panel, boxes extend from lower to upper quartile of data, whiskers show range. Orange horizontal line is plotted at the median. Blue circles are outliers. (For interpretation of the references to color in this figure legend, the reader is referred to the web version of this article.)

Pyramid Lake, and Death Valley (Lake Manly), or in the Altiplano-Puna plateau of the central Andes. The Eocene Green River Formation in Colorado could be another target for future work, particularly since they are rarely exposed in three dimensions (Awramik and Buchheim, 2015; Jagniecki et al., 2021). That is, for more ancient tufa, texture may be one of the only properties available for investigating these deposits.

Applying this method to other basins would require comparable numbers of images from all basins considered (i.e. hundreds of images). Given a basin with enough tufa outcrop to produce such a data set, a similar procedure to that presented in this paper would be performed. Whether or not images from different basins clustered together or apart would inform the viability of tufa texture as a proxy across basins. The parameterization of the algorithm or algorithms used would need to be adjusted to suit the expanded data set, including allowing for the possibility of different k values in k-means. However, diversifying the data set with a set of images from a totally distinct watershed, one whose chemistry is known to be distinct from others in the data set (i.e. Mono), would allow for a more thorough testing of the hypothesis that a different lake chemistry produces different textures of tufa. If comparable tufa textures are found across multiple lake systems, that texture could be indicative of a comparable growth environment between basins, at the time of deposition of the tufa. This information would allow for the tufa texture to be used as a direct proxy of lake chemistry and, in turn, depth.

Similarly, analyses like the one above would be made more rich with the inclusion of other environmental data. With the addition of data from more modern lakes, it would be possible to compare tufa texture to direct measurements of lake chemistry (e.g. alkalinity). Though beyond the scope of this study, future works could perform these kinds of analyses at Mono Lake. In older tufa, it could be revealing to compare tufa texture to the other proxies (e.g. Sr isotopes for groundwater). This work was limited to physical measurements in the field, but future works could improve upon it by including other basins or types of data, with the ultimate goal of using tufa texture as a proxy for depth in paleolakes.

6. Conclusions

The finding that the tufa at Mono are most visually similar to the columnar facies at Searles, and that the columnar facies is found most commonly at sites in Searles where tufa towers are also found, suggests that the response to question 1) posed above ("Is a particular facies of tufa at Searles objectively visually similar to those at Mono?") is that there is reasonable basis for the columnar facies being analogous to the tufa found at Mono Lake. In the context of past work, this study suggests a more abiotic, Mono-like origin for the Searles tufa, particularly in sites where columnar tufa can be found. That is, if the tufa at Mono are representative of the endmember spring-contribution facies, then these results would imply that a higher prevalence of columnar tufa is indicative of a greater spring contribution. This is a step towards the goal of tying tufa texture to formation environment.

The findings above do not exclude the possibility of a biological mechanism contributing to the formation of the tufa at Searles, but they also do not validate it. Thus, this study cannot recommend any biologically-based assumptions about the depth at which the tufa at Searles Valley formed. Future work is certainly needed to solidify these results. However, this work demonstrates that, with some tuning, machine learning studies of this kind have the potential to be useful in gleaning rich information from the geologic past. Considering images as 2-dimensional data that can be plotted and utilizing clustering methods allows for more rich comparisons of geologic images and their environment.

Machine learning and computer vision methods such as the ones used in this paper have the potential to draw further information from the geologic record than has previously been possible. As demonstrated here, these methods have the ability to represent data differently: images can be plotted by similarity, visual trends in facies can be quantified. By pursuing these new avenues of interrogating the geologic record, the geologic community has the potential to uncover new information from data sets and formations that have already been investigated with other techniques. Machine learning, in combination with more traditional methods and in the context of past research, can thus be a tool for deepening understanding of the Earth's past.

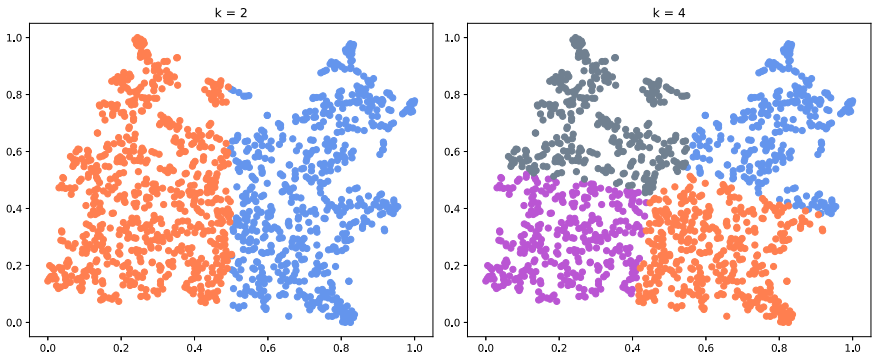

Fig. A.1. Clusters derived using $k = 2$ and $k = 4$.

7. Land acknowledgment

The field work for this study took place on the unceded land of the Newe (Western Shoshone) and the Monache (Western Mono) people. These lands are referred to above as Searles Valley and Mono Lake, respectively. Computational work was performed on the unceded territory of the Wampanoag Nation. The authors acknowledge the painful history of genocide and forced removal that these people have experienced, and recognize that the information gathered in this study cannot and should not supplant Indigenous ways of knowing the land.

CRediT authorship contribution statement

Michaela Fendrock: Conceptualization, Data curation, Formal analyses, Funding acquisition, Investigation, Methodology, Project administration, Software, Visualization, Writing – original draft, Writing – review & editing. **Christine Y. Chen:** Conceptualization, Resources, Writing – review & editing. **Kristian J. Olson:** Conceptualization, Investigation, Writing – review & editing. **Tim K. Lowenstein:** Conceptualization, Fund acquisition, Writing – review & editing. **David McGee:** Conceptualization, Fund acquisition, Project administration, Writing – review & editing.

Declaration of competing interest

The authors declare that they have no known competing financial interests or personal relationships that could have appeared to influence the work reported in this paper.

Acknowledgments

The authors would like to thank Anna Meurer for her important work in assessing the utility of various clustering metrics, and Divya Shanmugam for many helpful conversations about computer vision and appropriate algorithms. We would also like to thank Jade Brush for her continued and invaluable support in Searles Valley, and all members of 2020 SLAPP Field Trip for their help and discussion.

This work was supported primarily by a grant from the U.S. National Sciences Foundation (NSF-EAR-1903544 to DM, NSF-EAR-1903659 to TKL). Additionally, 2018 field work was funded from the Woods Hole Oceanographic Institution's Ocean Ventures Fund.

Code availability section

Repository name: tsne-nd

Contact: mfend@mit.edu, 978-460-0862

Hardware requirements: These scripts will run without a graphics card, but will be much more efficient with one. This was tested using a machine with a Nvidia GeForce GTX 1060.

Program language: Python

Software required: This program was tested with Tensorflow 2.2.0, Keras 2.4.3, Scikit-Learn 0.23.1, on Python 3.7.5

Program size: 5 KB

The source codes are available for downloading at the link: https://github.com/mfend/tsne-nd

Appendix. k-means sensitivity

Sensitivity analyses were performed for the value of k in clustering. These tests were performed upon the results of t-SNE as described in-text (perplexity = 18; 20,000 iterations). New clusters were found using each k = 2 and k = 4 (Fig. A.1). The 20 "endmembers" of each cluster (farthest from mean of data, as described in-text) were then visually inspected and assigned a facies (Table A.1, Table A.2). The composition of clusters for k = 2 and k = 4 were essentially the same: these clusters were not aligned with the facies as defined above (Fig. 2), indicating that the boundaries of these clusters were not defined by the boundaries between facies. k = 3 was thus the optimal choice of k for this study.

Table A.1
General distribution of facies between clusters using $k = 2$.

Cluster Number	Weathered Nodular	Columnar	Nodular	Porous
1	5	1	1	13
2	6	1	2	11

Table A.2
General distribution of facies between clusters using $k = 4$.

Cluster Number	Weathered Nodular	Columnar	Nodular	Porous
1	6	1	2	11
2	5	2	2	11
3	6	1	1	12
4	6	0	2	12

References

Abdelmoula, W.M., Balluff, B., Englert, S., Dijkstra, J., Reinders, M.J., Walch, A., McDonnell, L.A., Lelieveldt, B.P., 2016. Data-driven identification of prognostic tumor subpopulations using spatially mapped t-SNE of mass spectrometry imaging data. Proc. Natl. Acad. Sci. 113 (43), 12244–12249.

Alfeld, M., Pedetti, S., Martinez, P., Walter, P., 2018. Joint data treatment for vis–NIR reflectance imaging spectroscopy and XRF imaging acquired in the Theban Necropolis in Egypt by data fusion and t-SNE. C. R. Phys. 19 (7), 625–635.

Awramik, S.M., Buchheim, H.P., 2015. Giant stromatolites of the Eocene Green River formation (Colorado, USA). Geology 43 (8), 691–694.

Becht, E., Dutertre, C.A., Kwok, I.W., Ng, L.G., Ginhoux, F., Newell, E.W., 2018. Evaluation of UMAP as an alternative to t-SNE for single-cell data. 298430, bioRxiv.

Benson, L., 1994. Carbonate deposition, Pyramid Lake subbasin, Nevada: 1. Sequence of formation and elevational distribution of carbonate deposits (tufas). Palaeogeogr., Palaeoclimatol., Palaeoecol. 109 (1), 55–87.

Benson, L.V., Currey, D.R., Dorn, R.I., Lajoie, K.R., Oviatt, C.G., Robinson, S.W., Smith, G.I., Stine, S., 1990. Chronology of expansion and contraction of four Great Basin lake systems during the past 35,000 years. Palaeogeogr., Palaeoclimatol., Palaeoecol. 78 (3–4), 241–286.

Bischoff, J.L., Stine, S., Rosenbauer, R.J., Fitzpatrick, J.A., Stafford, Jr., T.W., 1993. Ikaite precipitation by mixing of shoreline springs and lake water, Mono lake, California, USA. Geochim. Et Cosmochim. Acta 57 (16), 3855–3865.

Brasier, A., Wacey, D., Rogerson, M., Guagliardo, P., Saunders, M., Kellner, S., Mercedes-Martin, R., Prior, T., Taylor, C., Matthews, A., et al., 2018. A microbial role in the construction of mono lake carbonate chimneys? Geobiology 16 (5), 540–555.

Broecker, W.S., Orr, P.C., 1958. Radiocarbon chronology of lake Lahontan and Lake Bonneville. Geol. Soc. America Bull. 69 (8), 1009–1032.

Candy, I., Schreve, D., 2007. Land–sea correlation of middle pleistocene temperate substages using high-precision uranium-series dating of tufa deposits from southern England. Quat. Sci. Rev. 26 (9–10), 1223–1235.

Celik, T., 2009. Unsupervised change detection in satellite images using principal component analysis and k-means clustering. IEEE Geosci. Remote Sens. Lett. 6 (4), 772–776.

Council, T.C., Bennett, P.C., 1993. Geochemistry of ikaite formation at Mono Lake, California: Implications for the origin of tufa mounds. Geology 21 (11), 971–974.

DeMott, L.M., Napieralski, S.A., Junium, C.K., Teece, M., Scholz, C.A., 2020. Microbially influenced lacustrine carbonates: A comparison of late quaternary lahontan tufa and modern thrombolite from Fayetteville Green Lake, NY. Geobiology 18 (1), 93–112.

Dunn, J.R., 1953. The origin of the deposits of tufa in Mono Lake [California]. J. Sediment. Res. 23 (1), 18–23.

Fang, M., Li, X., 2019. An artificial neural networks-based tree ring width proxy system model for paleoclimate data assimilation. J. Adv. Modelling Earth Syst. 11 (4), 892–904.

Ford, T., Pedley, H., 1996. A review of tufa and travertine deposits of the world. Earth-Sci. Rev. 41 (3–4), 117–175.

Guo, X., Chafetz, H.S., 2012. Large tufa mounds, Searles Lake, California. Sedimentology 59 (5), 1509–1535.

Guo, X., Chafetz, H.S., 2014. Trends in δ18o and δ13C values in lacustrine tufa mounds: Palaeohydrology of Searles Lake, California. Sedimentology 61 (1), 221–237.

Hostetler, S.W., Bartlein, P.J., 1990. Simulation of lake evaporation with application to modeling lake level variations of Harney-Malheur Lake, Oregon. Water Resour. Res. 26 (10), 2603–2612.

Huntingford, C., Jeffers, E.S., Bonsall, M.B., Christensen, H.M., Lees, T., Yang, H., 2019. Machine learning and artificial intelligence to aid climate change research and preparedness. Environ. Res. Lett. 14 (12), 124007.

Jagniecki, E.A., Lowenstein, T.K., Demicco, R.V., Baddouh, M., Carroll, A.R., Beard, B.L., Johnson, C.M., 2021. Spring origin of eocene carbonate mounds in the Green River formation, Northern Bridger Basin, Wyoming, USA. Sedimentology.

Jayko, A.S., Forester, R.M., Kaufman, D.S., Phillips, F.M., Yount, J., McGeehin, J., Mahan, S.A., Reheis, M., Hershler, R., Miller, D., 2008. Late Pleistocene lakes and wetlands, Panamint Valley, Inyo County, California. Spec. Pap.-Geol. Soc. America 439, 151.

Kanungo, T., Mount, D.M., Netanyahu, N.S., Piatko, C.D., Silverman, R., Wu, A.Y., 2002. An efficient k-means clustering algorithm: Analysis and implementation. IEEE Trans. Pattern Anal. Mach. Intell. 24 (7), 881–892.

Kaufman, A., Broecker, W., 1965. Comparison of Th230 and C14 ages for carbonate materials from Lakes Lahontan and Bonneville. J. Geophys. Res. 70 (16), 4039–4054.

Klimczak, L.J., von Eschenbach, C.E., Thompson, P.M., Buters, J.T., Mueller, G.A., 2020. Mixture analyses of air-sampled pollen extracts can accurately differentiate pollen taxa. Atmos. Environ. 243, 117746.

Kobak, D., Berens, P., 2019. The art of using t-SNE for single-cell transcriptomics. Nature Commun. 10 (1), 1–14.

Kobak, D., Linderman, G.C., 2019. UMAP does not preserve global structure any better than t-SNE when using the same initialization. bioRxiv.

Ku, T.L., Luo, S., Lowenstein, T.K., Li, J., Spencer, R.J., 1998. U-series chronology of lacustrine deposits in Death Valley, California. Quat. Res. 50 (3), 261–275.

Li, W., Cerise, J.E., Yang, Y., Han, H., 2017. Application of t-SNE to human genetic data. J. Bioinf. Comput. Biol. 15 (04), 1750017.

Linderman, G.C., Steinerberger, S., 2019. Clustering with t-SNE, provably. SIAM J. Math. Data Sci. 1 (2), 313–332.

Munroe, J.S., Laabs, B.J., 2013. Temporal correspondence between pluvial lake highstands in the southwestern US and Heinrich event 1. J. Quat. Sci. 28 (1), 49–58.

Njock, P.G.A., Shen, S.L., Zhou, A., Lyu, H.M., 2020. Evaluation of soil liquefaction using AI technology incorporating a coupled ENN/t-SNE model. Soil Dyn. Earthq. Eng. 130, 105988.

Palacio Niño, J.O., Berzal, F., 2019. Evaluation metrics for unsupervised learning algorithms. arXiv preprint arXiv:1905.05667.

Pedregosa, F., Varoquaux, G., Gramfort, A., Michel, V., Thirion, B., Grisel, O., Blondel, M., Prettenhofer, P., Weiss, R., Dubourg, V., et al., 2011. Scikit-learn: Machine learning in python. J. Mach. Learn. Res. 12, 2825–2830.

Peng, T.H., Goddard, J., Broecker, W., 1978. A direct comparison of 14C and 230Th ages at Searles Lake, California1. Quat. Res. 9 (3), 319–329.

Pérez-Ortiz, M., Durán-Rosal, A.M., Gutiérrez, P.A., Sánchez-Monedero, J., Nikolaou, A., Fernández-Navarro, F., Hervás-Martínez, C., 2019. On the use of evolutionary time series analysis for segmenting paleoclimate data. Neurocomputing 326, 3–14.

Petryshyn, V.A., Rivera, M.J., Agić, H., Frantz, C.M., Corsetti, F.A., Tripati, A.E., 2016. Stromatolites in Walker Lake (Nevada, Great Basin, USA) record climate and lake level changes˜35,000 years ago. Palaeogeogr., Palaeoclimatol., Palaeoecol. 451, 140–151.

Pouyet, E., Rohani, N., Katsaggelos, A.K., Cossairt, O., Walton, M., 2018. Innovative data reduction and visualization strategy for hyperspectral imaging datasets using t-SNE approach. Pure Appl. Chem. 90 (3), 493–506.

Scholl, D.W., 1960. Pleistocene algal pinnacles at Searles Lake, California. J. Sediment. Res. 30 (3), 414–431.

Scholl, D.W., Taft, W.H., 1964. Algae, contributors to the formation of calcareous tufa, Mono Lake, California. J. Sediment. Res. 34 (2), 309–319.

Shearman, D., McGugan, A., Stein, C., Smith, A., 1989. Ikaite, CaCO3ś6H2O, precursor of the thinolites in the quaternary tufas and tufa mounds of the Lahontan and Mono Lake Basins, western United States. Geol. Soc. America Bull. 101 (7), 913–917.

Smith, G.I., 2009. Late Cenozoic Geology and Lacustrine History of Searles Valley, Inyo and San Bernardino Counties, California. US Geological Survey.

Stine, S., 1990. Late holocene fluctuations of Mono Lake, eastern California. Palaeogeogr., Palaeoclimatol., Palaeoecol. 78 (3–4), 333–381.

Van der Maaten, L., Hinton, G., 2008. Visualizing data using t-SNE. J. Mach. Learn. Res. 9 (11).

Vorster, P., 1985. A Water Balance Forecast Model for Mono Lake, California (Master's thesis). Calif. State University, Hayward.

Wattenberg, M., Viégas, F., Johnson, I., 2016. How to use t-SNE effectively. Distill 1 (10), e2.